Differentiation trajectories of the *Hydra* nervous system reveal transcriptional regulators of neuronal fate

Abby S Primack[a], Jack F Cazet[a], Hannah Morris Little[a], Susanne Mühlbauer[b], Ben D Cox[a], Charles N David[c], Jeffrey A Farrell[d], Celina E Juliano[a*]

[a] Department of Molecular and Cellular Biology, University of California, Davis, CA 95616

[b] Department of Plant Biochemistry, Ludwig-Maximilians-University Munich, 82152 Planegg-Martinsried, Germany

[c] Department of Biology, Ludwig-Maximilians-University Munich, 82152 Martinsried, Germany

[d] Division of Developmental Biology, *Eunice Kennedy Shriver* National Institute of Child Health and Human Development, Bethesda, MD 20814, USA

*Corresponding Author

Email: cejuliano@ucdavis.edu

ABSTRACT

The small freshwater cnidarian polyp *Hydra vulgaris* uses adult stem cells (interstitial stem cells) to continually replace neurons throughout its life. This feature, combined with the ability to image the entire nervous system (Badhiwala et al., 2021; Dupre & Yuste, 2017) and availability of gene knockdown techniques (Juliano, Reich, et al., 2014; Lohmann et al., 1999; Vogg et al., 2022), makes *Hydra* a tractable model for studying nervous system development and regeneration at the whole-organism level. In this study, we use single-cell RNA sequencing and trajectory inference to provide a comprehensive molecular description of the adult nervous system. This includes the most detailed transcriptional characterization of the adult *Hydra* nervous system to date. We identified eleven unique neuron subtypes together with the transcriptional changes that occur as the interstitial stem cells differentiate into each subtype. Towards the goal of building gene regulatory networks to describe *Hydra* neuron differentiation, we identified 48 transcription factors expressed specifically in the *Hydra* nervous system, including many that are conserved regulators of neurogenesis in bilaterians. We also performed ATAC-seq on sorted neurons to uncover previously unidentified putative regulatory regions near neuron-specific genes. Finally, we provide evidence to support the existence of transdifferentiation between mature neuron subtypes and we identify previously unknown transition states in these pathways. All together, we provide a comprehensive transcriptional description of an entire adult nervous system, including differentiation and transdifferentiation pathways, which provides a significant advance towards understanding mechanisms that underlie nervous system regeneration.

INTRODUCTION

Understanding the fundamental principles of nervous system regeneration is key to developing treatments for traumatic brain injury, spinal cord injury, and neurodegenerative diseases. Most well-established neurobiology research organisms are not able to replace adult neurons, making their utility for investigating adult nervous system regeneration limited. By contrast, the small freshwater cnidarian polyp *Hydra vulgaris* (Fig 1A) has active adult multipotent stem cells that renew its entire nervous system throughout its life (David & Gierer, 1974). In addition, the relative simplicity of *Hydra* allows for the study of adult nervous system development and regeneration at the level of the entire nervous system. *Hydra* has a relatively simple and well-understood body that is composed of two epithelial monolayers, an outer ectodermal layer and an inner endodermal layer. The nervous system is made up of approximately 3,000-5,000 neurons (about 3-5% of all cells in the body) arranged into two separate nerve nets that are embedded in the two epithelial layers (Keramidioti et al., 2023). *Hydra* neurons are part of the interstitial cell lineage (David, 2012; David & Murphy, 1977) and are supported by multipotent adult interstitial stem cells (ISCs) that are found in the interstices of the ectodermal epithelial body column cells (Fig 1B). Due to passive tissue displacement towards the extremities that result in perpetual cell loss (Fig 1A arrows), the ISCs continuously replace neurons (Campbell, 1967; David & Gierer, 1974; Hager & David, 1997) such that all neural differentiation pathways are active in the adult polyp and are therefore accessible for experimentation. The ISCs also enable regeneration of the entire nervous system following injury.

In addition to exhibiting continual, widespread neuronal regeneration, *Hydra* are amenable to genetic manipulations, such as gene knock-down through the expression of RNA hairpins (Juliano, Reich, et al., 2014; Lohmann et al., 1999) or the electroporation of siRNAs (Lohmann et al., 1999; Vogg et al., 2022). Additionally, it is straightforward to create stable transgenic *Hydra* lines using cell-type-specific promoters (Dupre & Yuste, 2017; Klimovich et al., 2019; Siebert et al., 2019; Wittlieb et al., 2006). Taken together, these attributes make *Hydra* an accessible model for neurobiology, enabling us to test the developmental regulators of neuron differentiation for an entire nervous system. Finally, *Hydra*'s position on the phylogenetic tree

as a member of Cnidaria, the sister group to bilaterians, enables researchers to explore the evolution of the molecular mechanisms underlying nervous system development and regeneration.

Decades of research provide a basic framework for *Hydra* neurobiology, including the source of new neurons (David, 2012), the relative distribution of the nervous system along the oral-aboral axis (H. Bode et al., 1973), and the rates of neurogenesis in an uninjured *Hydra* (David & Gierer, 1974). As part of our previous study creating a whole animal single cell expression map, we transcriptionally profiled *Hydra* neurons and determined their spatial location (Siebert et al., 2019). However due to the relatively small number of neurons sequenced (~3,500), it remained unclear whether we successfully profiled all populations of differentiated neurons. Additionally, in our original study we did not capture enough intermediate states of neuronal differentiation or transdifferentiation to properly resolve the transcriptional changes that occur as neurons are produced during homeostatic maintenance.

We resolved these issues by increasing our data set by 10-fold to ~35,000 single-cell transcriptomes of neurons and neural progenitors. From these data, we identified eleven neuron subtypes in *Hydra*: three in the endodermal nerve net and eight in the ectodermal nerve net. These data are largely consistent with our previously published spatial molecular map of the *Hydra* nervous system (Siebert et al., 2019). We used our data to build differentiation trajectories describing the transcriptional changes that underlie the homeostatic differentiation of all eleven neuron subtypes in *Hydra*. We also provide new evidence to support widespread transdifferentiation between neuron subtypes in the *Hydra* nervous system. We performed neuron-enriched Assay for Transposase-Accessible Chromatin (ATAC-seq) (Buenrostro et al., 2013; Corces et al., 2017) to identify the chromatin states of *Hydra* neurons, and we identified the transcription factors that are expressed during the differentiation of all *Hydra* neuron subtypes. Our data describe the differentiation of a complete nervous system and identify putative key regulators of each neuronal subtype for future testing. Furthermore, our data lay the groundwork for studies investigating how these pathways are activated to regenerate the *Hydra* nervous system in response to injury.

RESULTS

The *Hydra* nervous system is composed of eleven transcriptionally distinct neuron subtypes

In our previous study, we used Drop-seq (Macosko et al., 2015) to build a single cell atlas of the adult *Hydra* polyp, which included approximately 3,500 single-cell transcriptomes of differentiated neurons and cells undergoing neurogenesis (Siebert et al., 2019). In this present study, we first aimed to increase the number of neural single-cell transcriptomes to reveal any molecular diversity in the *Hydra* neuron repertoire that we may have previously missed due to the relatively low number of cells sequenced. To this end, we used scRNA-seq (10x Genomics) to increase the number of sequenced neurons and neural progenitors to ~35,000 single-cell transcriptomes.

To enrich for neurons and neural progenitors, we used Fluorescent Activated Cell Sorting (FACS) to collect cells from two different transgenic lines: (1) *Tg(actin1:GFP)*$^{rs3\text{-}in}$, in which GFP is expressed in all differentiated neurons, neural progenitors, and ISCs (Keramidioti et al., 2023), and (2) *Tg(tba1c:mNeonGreen)*$^{cj1\text{-}gt}$, which was created for this study and in which mNeonGreen is predicted to be expressed in all differentiated neurons (Fig S1, S2; Table S1). We combined our new data with the neuronal single-cell transcriptomes we previously collected (Siebert et al., 2019) for downstream processing (Table S2). For all libraries, the sequencing reads were mapped to the *Hydra vulgaris* strain AEP gene models (Cazet et al., 2023) and processed following standard procedures (Fig S3) (Macosko et al., 2015). After filtering, we recovered 35,071 single-cell neural transcriptomes with a detected median of 1371.5 genes and 2887.5 UMIs per cell (Table S2). This is in comparison to the detected median of 563.5 genes and 1082 UMIs per cell in the neuron-enriched libraries collected by Drop-seq in our previous study (Siebert et al., 2019).

To identify distinct neuron subtypes in our data set, we used Seurat to perform Louvain clustering and visualized the results using Uniform Manifold Approximation and Projection (UMAP) (Fig 1C) (Hao et al., 2021; McInnes et al., 2018; Satija et al., 2015; Stuart et al., 2019). We recovered and annotated 11 neural clusters using marker genes identified previously

(Siebert et al., 2019): three neuron subtypes that reside in the endodermal nerve net (en1, en2, and en3) and eight neuron subtypes that reside in the ectodermal nerve net (ec1A, ec1B, ec2, ec3A, ec3B, ec3C, ec4, and ec5) (Fig 1 C,D, Fig S4, Table S3). We also recovered three clusters that express marker genes for multiple subtypes that we hypothesize are in a transition state (td1, td2, td3) (discussed further below). We also annotated stem cell and neural progenitor cell clusters using markers from our previous study (Siebert et al., 2019).

This analysis aligned with our previously published map (Siebert et al., 2019) with one small discrepancy regarding the previously annotated ec4A and ec4B neuron subtypes. Although ec4A and ec4B clustered separately in our previously published map, it is unclear if this distinction is justified in our current analysis and we therefore have collapsed this into a single ec4 population. Future work should more carefully define this population on morphological and functional levels. Finally, we performed non-negative matrix factorization (NMF) (Kotliar et al., 2019) to identify groups of co-expressed genes ("metagenes"), and we recovered at least one metagene for each of the eleven neuron subtypes, as well as for the three newly annotated transdifferentiation cell states (Fig S5).

In summary, our new scRNA-seq data set enabled us to achieve deeper sequencing, significantly increase the number of neural progenitor transcriptomes, and profile rarer populations of cells potentially undergoing transdifferentiation. Below, we use these data to profile the transcription factors expressed in the entire nervous system and resolve stem cell differentiation and transdifferentiation trajectories.

Comprehensive identification of transcription factors selectively expressed in the *Hydra* nervous system

Our work makes *Hydra* one of the few adult organisms in which the entire nervous system has been transcriptionally defined. Given the relative simplicity of only 11 neuron subtypes, *Hydra* provides the opportunity to build gene regulatory networks (GRNs) that describe the differentiation of all neurons in an adult nervous system. This requires both identifying the

transcription factors (TFs) expressed during nervous system development as well as determining the cis-regulatory elements (CREs) that are bound by those TFs. To provide starting points for this long-term goal, we used our scRNA-seq data sets to identify the TFs expressed in the *Hydra* nervous system, but not in other cell types.

In our previous work, we identified 811 putative transcription factors (TFs) (i.e., genes with predicted DNA binding domains) with detectable expression in *Hydra* polyps (Cazet et al., 2023). Here, we find that 48 of these TFs are selectively expressed in the *Hydra* nervous system (Fig 2, Fig S6). Of these 48 TFs, four are expressed in neural progenitors (*myc3, myb, rfx5/7, hmgb3*); five are expressed in different endodermal neurons (neurog1/2/3*, G004963, duxa/b, klf3, ptf1a*); 12 are expressed in different ectodermal neurons (*smad4, sox3, foxl2, zic1/2/3/4/5, litaf, G018876, noto, sox2, arx, bhlha15, gata3, ndf1, G010046*) and the remainder are either co-expressed in ectodermal and endodermal neurons or are pan-neuronally expressed.

As mentioned above, building GRNs to describe nervous system development in *Hydra* will also require determining CREs that are bound by the neural TFs. As a first step towards this goal, we performed ATAC-seq on FACS-sorted *Hydra* neurons from the *Tg(actin1:GFP)*$^{rs3\text{-}in}$ and *Tg(tba1c:mNeonGreen)*$^{cj1\text{-}gt}$ transgenic lines to reveal the cis-regulatory landscape of *Hydra* neurons (Table S4). The data produced were high quality (based on ENCODE standards, (encodeproject.org/atac-seq) (Landt et al., 2012)), and replicates exhibited high reproducibility (Fig S7). Data quality was similar to three previously published whole *Hydra vulgaris* strain AEP ATAC-seq data sets (Cazet et al., 2023), suggesting that FACS sorting did lower the quality of the nuclei collected.

We found that peaks from the neuronal ATAC-seq libraries collected from both transgenic lines had significantly increased accessibility near neural genes as compared to whole animal ATAC-seq data ($p < 0.001$ for each line; Fig 3A-B). Peak accessibility near some neuronal subtype-specific genes varied between samples generated from different transgenic lines but reflected the cell types collected from those transgenic lines (Fig S8). Notably, these data identified

accessible regions near neuronal genes that were not detected in our previously collected whole-animal data (Cazet et al., 2023), which demonstrates the utility of these data for identifying the regulatory regions that drive neuronal expression (Figure 3C-H).

Differentiation trajectories reveal transition states during development of an entire nervous system

Having defined the repertoire of neuron subtypes in *Hydra*, as well as having identified the transcription factors selectively expressed in the nervous system, we next aimed to determine the ordering of transcription factor expression over developmental time. The *Hydra* nervous system undergoes continual renewal with complete nervous system turnover approximately every three weeks (H. R. Bode et al., 1988). Therefore, when performing scRNA-seq on the adult *Hydra*, we expect to profile stem cells, differentiated cells, and cells in various states of the differentiation process (Siebert et al., 2019). Thus, we used our scRNA-seq data to build differentiation trajectories for each of the 11 neuron subtypes using URD (Fig 4A), which is a diffusion-based approach to generate developmental trajectories in the form of branching trees (Farrell et al., 2018). URD requires that we define both the root and the tips of the tree. In this case, the root is ISCs, which were defined by a specific marker (*G002332*) (Siebert et al., 2019), and the tips were the neuron subtypes as defined by their expression of specific markers (Fig S4) and lack of progenitor markers.

Our previous work showed that as ISCs begin the process of neurogenesis, they express the transcription factors *myc3* (*G003730*) and *myb* (*G020130*); the expression of these genes is lost as neurons complete differentiation (Siebert et al., 2019). Therefore, we used the expression of *myc3* and *myb* to identify the neural progenitors in our trajectory analysis and found that two populations of cells expressing both *myc3* and *myb* initially split from the ISCs. One of these progenitor populations (Fig 4A, segment 3) gives rise to all endodermal neurons (en1, en2, en3) and the other (Fig 4A segment 2) gives rise to most ectodermal neurons (ec1A, ec1B, ec2, ec3A, ec3B, ec3C, ec4). Intriguingly, the ec5 ectodermal neurons (Fig 4A segment 19) did not connect to either of these populations and rather appeared to differentiate directly from ISCs. This

suggests that these neurons may either differentiate directly, which would be surprising (David, 2012), or that there is an additional progenitor population or transition state that was not captured in our data set. Regardless, our data reveal that most endodermal and ectodermal neurons likely arise from two distinct progenitor populations. As differentiation proceeds, neural progenitors become more restricted in fate potential, ultimately giving rise to the eleven neuron subtypes.

The differentiation trajectory also allows us to track TF dynamics over developmental time. To visualize this, we plotted the temporal expression of genes, with a focus on TFs, that are expressed during the differentiation of each neuron subtype. For example, we tracked the expression of genes *bhlha15 (G021353)*, *gata3 (G022640), hym355 (G004115)*, and ec3A marker *G021930* over the course of ec3A differentiation (Fig 4A segments 1, 2, 4, 11, Fig 4B). To validate the transition states that our trajectory predicts for ec3A differentiation, we used double fluorescent *in situ* hybridization (FISH), focusing on pairs of genes with overlapping expression domains during three predicted transition states of ec3A differentiation (Fig 4C-U). For each pair of genes (Fig 4C-G *bhlha15* + *gata3*, Fig 4H-L *gata3* + *hym355*, Fig 4M-Q *hym355* + *G021930*), we found cells that individually expressed the genes as well as cells that co-expressed the pair of genes, as predicted by our differentiation trajectory. We also found the majority of stained neurons co-expressing *hym355* + *G021930* in the aboral end (Fig 4M, R-U), which is where we expect to find ec3A neurons. This confirms that our trajectory analysis identified the dynamics of gene expression during the specification and differentiation of individual neuronal subtypes in *Hydra*.

Transcriptional evidence of neuron transdifferentiation in *Hydra*

Although our trajectory analysis identified the dynamics of gene expression when new neurons are born from ISCs, our data also revealed strong evidence of transdifferentiation between differentiated neuron subtypes. Due to the tissue dynamics in *Hydra* (Fig. 1A,D), neurons are continually displaced towards the extremities, which has led to speculation that neurons undergo transdifferentiation to accommodate their new position (H. R. Bode, 1992). Some

studies have documented neuron transdifferentiation in *Hydra*, but these studies were done in animals that lacked ISCs (H. R. Bode, 1992; Koizumi et al., 1988; Koizumi & Bode, 1986, 1991). *Hydra* lacking ISCs would be unable to make neurons *de novo* and may thus be forced to activate normally unused developmental pathways. We therefore looked for evidence of neuronal transdifferentiation in our data set to determine if this was a common phenomenon in unmanipulated *Hydra*. In addition to the eleven previously identified neuron subtypes, we found three additional clusters [annotated as transdifferentiation (td) 1, 2, and 3] (Fig 1C). We hypothesize that these clusters represent neurons in the process of transdifferentiation because they express markers of multiple previously identified neuron subtypes. Based on the co-expression of ec1A and ec1B markers (Fig 5A), we hypothesize that transdifferentiation clusters 1 and 3 represent ec1A neurons from the body column transdifferentiating into ec1B neurons as they are displaced toward the oral end. Based on the co-expression of ec1A and ec5 markers (Fig 5A), we hypothesize that the transdifferentiation cluster 2 represents ec1A neurons from the body column transdifferentiating into ec5 peduncle neurons as they are displaced toward the aboral end.

To uncover possible transdifferentiation events**,** we visualized cellular relationships in a structure agnostic manner as a complementary approach to URD using a Force Directed Layout (FDL) (a structure agnostic program) as a complementary approach to URD (Farrell et al., 2018; Fruchterman & Reingold, 1991). We isolated groups of neurons that we hypothesized undergo transdifferentiation with each other and generated Force Directed Layouts (FDLs) based on weighted k-nearest neighbor networks, where linkages were stronger when cells were more transcriptionally similar (Fruchterman & Reingold, 1991; Jacomy et al., 2014) (Fig 5B-D). Although not demonstrated directly in the data, we inferred the directionality of transdifferentiation events in this analysis based on the known direction of cell movements (from the body column toward extremities) and the anatomical location of individual neuronal populations (Fig 1D, Fig 5B-D). For the first group of cells (ec1A, ec1B, ec5, td1, td2, td3), we found that ec1A connects to ec1B through two intermediate transdifferentiation populations (td1 and td3) (Fig 5B). Additionally, we found that ec1A weakly connects to ec5 both directly and possibly through an intermediate state of td2, although the relationship of td2 to ec1A and

ec5 is less clear . This provides further evidence that body column ec1A cells transdifferentiate into head ec1B cells, and possibly peduncle ec5 neurons. For the second group of cells, (ec3A, ec3B, ec3C, ec3_precursors), ec3A and ec3C appear to be derived from ec3 precursors in addition to undergoing transdifferentiation from body column ec3B neurons as they move into the extremities (Fig 5C). As a control, we tested the interactions of several neuron subtypes with little to no predicted transcriptional similarity (Fig 5D). As expected, there were no strong connections between the control clusters.

DISCUSSION

The number of research organisms used to study nervous system development and function has substantially increased in recent years due to advances in sequencing technology (Albertin et al., 2022; Fincher et al., 2018; Hulett et al., 2020, 2022; Orvis et al., 2022; Sachkova et al., 2021; Sebé-Pedrós et al., 2018). This has enabled researchers to characterize the transcriptional diversity in neurons from a wide range of organisms. However, very few comprehensive transcriptional descriptions of adult nervous systems currently exist. Here, we provide a transcriptional analysis of the entire *Hydra vulgaris* nervous system. Although *Hydra* shares many of the same experimental advantages as well-established invertebrate models, such as small size, optical transparency, and ability to test gene function, it is also able to regenerate its entire nervous system from adult stem cells (H. R. Bode et al., 1988; Dupre & Yuste, 2017). We built a molecular map of the *Hydra* nervous system using approximately 35,000 neural single cell transcriptomes, including differentiated neurons and cells undergoing neurogenesis. We surveyed for previously undetected diversity, and in addition to confirming 11 neuron subtypes (Siebert et al., 2019), we identified the first transcriptional evidence of neurons undergoing transdifferentiation in *Hydra*. We identified putative transcriptional regulators for all subtypes, performed ATAC-seq to identify the chromatin state of *Hydra* neurons, and built differentiation trajectories describing the transcriptional changes that underlie *Hydra* neurogenesis. This work represents the most detailed molecular description of the adult *Hydra* nervous system to date.

These results build on the work started in our previously published molecular map of the *Hydra* nervous system (Siebert et al., 2019). We increased the number of sequenced cells ten-fold and confidently identified 11 neuron subtypes. The number of identified subtypes has remained stable after increasing the number of profiled cells substantially, which suggests that our data reveals the entire complement of transcriptionally distinct neuron subtypes present in *Hydra*. Our neuron subtype analysis is also consistent with an scRNA-seq study from the Bosch lab in which approximately 1000 neurons were sequenced (Klimovich et al., 2020). A benefit of our larger data set is the higher capture rate of transition states (which are rare as compared to differentiated neurons), enabling a more complete reconstruction of the developmental trajectories that give rise to different neuronal subpopulations. For instance, we identified three transdifferentiation states: transdifferentiation clusters (td) 1, 2, and 3. In addition to identifying individual metagenes for each of these transdifferentiation populations (Fig S5), cells from each transdifferentiation population were sequenced in all 16 libraries, suggesting that these are biologically valid cells rather than a library-specific batch effect. Our favored hypothesis is that these clusters represent ec1A cells in the body column that are undergoing transdifferentiation into either ec1B cells at the oral end or ec5 cells at the aboral end. This hypothesis is supported by our findings from the FDL analysis (Fig 5). The ability of neurons to transdifferentiate has been previously shown in *Hydra* that lack ISCs (Koizumi et al., 1988; Koizumi & Bode, 1986, 1991), but this is the first evidence that this phenomenon occurs as part of the normal homeostatic maintenance of the *Hydra* nervous system.

Our analysis identified marker genes of all neuron subtypes as well as different progenitor states (Fig S4), which will enable the creation of reporter lines to interrogate nervous system development and regeneration in future studies. The new, neuron-enriched ATAC-seq data generated in this study will facilitate this effort by enabling the accurate identification of regulatory regions. For instance, in this study, we created a new mNeonGreen reporter line using the regulatory region of *tba1c (G019559*), which is predicted to be expressed pan-neuronally (Fig 3D-E). However, despite transmission through the germline, we found that *Tg(tba1c:mNeonGreen)*$^{cj1\text{-}gt}$ did not express mNeonGreen uniformly in all neurons, suggesting

that we did not capture the full regulatory region of *tba1c* (for validation of line, see Fig S2). When making this line, we used peaks from the whole animal 105 ATAC-seq data (Siebert et al., 2019) as a guide for identifying the regulatory region and cloned 1901 bp upstream of the *tba1c* transcription start site (TSS). Our new neuron-enriched ATAC-seq data identifies an additional peak ~3,000 bp upstream of the TSS that was not captured in our cloning process (Fig S2N). This missing element of the regulatory region could explain why we do not have uniform transgene expression across the *Hydra* nervous system in our *Tg(tba1c:mNeonGreen)*$^{cj1\text{-}gt}$ line. This demonstrates the utility of our neuron-enriched ATAC-seq libraries, which provide novel information about the regulatory regions of neuronal genes and will help guide the design of neuronal promoter lines in the future. As we have identified specific gene markers for every neuron subtype, this will ultimately allow us to create transgenic reporter lines for each neuron subtype and individually analyze the regulatory regions of each of *Hydra's* 11 neural subtypes.

We have uncovered the molecular underpinnings of the entire *Hydra* nervous system, including 48 TFs that are expressed only in neurons or neuronal progenitors (Fig 2, Fig S6). This includes TFs that are common to all neurons as well as more selectively expressed TFs that are likely involved in the specification of individual neuron subtypes. These TFs are representative of many TF families, such as: C2H2 Zinc Finger family (10/48), bHLH superfamily (8/48), Winged Helix superfamily (4/48), Homeobox family (4/48), high mobility group box superfamily (3/48), SMAD family (3/48), bZIP family (2/48), Bed-type Zinc Finger family (2/48), and GATA-type Zinc Finger family (1/48). Many of these TFs are also conserved in bilaterian neurogenesis pathways, including: *myc3* (*G003730*) (Knoepfler et al., 2002)*, neurog1/2/3 (G008286)* (Blader et al., 1997; Lee, 1997)*, sox3 (G001357)* (Bylund et al., 2003; Rogers et al., 2013)*, ndf1 (G011383)* (Lee et al., 1995; Miyata et al., 1999)*, atoh8 (G021588)* (Jarman et al., 1993)*, and creb1 (G019837)* (Dworkin et al., 2007). This suggests their conserved role in regulating nervous system development in the last common ancestor of bilaterians and cnidarians.

We observed differences in TF expression patterns between endodermal and ectodermal neurons that may reflect different developmental strategies. The three endodermal neural subtypes (en1, en2, and en3) each selectively express one or two TFs (Fig 2), suggesting that

these TFs act as terminal selectors of the endodermal neural states; this is a similar strategy described for specification of *C. elegans* neurons (Doitsidou et al., 2018; Hobert, 2016; Patel & Hobert, 2017). By contrast, ectodermal neurons express a larger number of neuron-specific TFs and while each subtype expresses a unique set of these TFs, ec2 is the only neuron subtype to express unique TFs (*G018876* and *noto*) (Fig 2). This suggests that the ectodermal neurons are specified by combinatorial gene control and may also reflect their capacity to transdifferentiate between ectodermal neuronal subtypes.

To better understand the specification of *Hydra* neurons, we performed trajectory inference using URD and built a branching differentiation trajectory to describe the process by which all 11 neurons develop from the multipotent ISCs (Fig 4A).Our data suggest that the first decision point of neuronal differentiation is the choice between endodermal and ectodermal fate. This may reflect the unique biology of these progenitors, given that the endodermal progenitor cells have to cross the ECM to populate the endodermal nerve net. Further, we note that groups of ectodermal neurons hypothesized to be part of the same neural circuits (RP1: ec3A, ec3B, ec3C and CB: ec1A, ec1B, ec5) (Dupre & Yuste, 2017; Keramidioti et al., 2023; Siebert et al., 2019) share progenitor states, with the exception of ec5.

All together, these data provide a comprehensive transcriptional description of the homeostatic *Hydra* nervous system. These data are a hypothesis generator and critical starting point for functional studies of nervous system development, regeneration, and function.

MATERIALS AND METHODS

***Hydra* Strains and Culturing Conditions**

Hydra vulgaris strains AEP, *Tg(actin1:GFP)*$^{rs3\text{-}in}$ (Keramidioti et al., 2023), and *Tg(tba1c:mNeonGreen)*$^{cj1\text{-}gt}$ were cultured in *Hydra* medium at 18°C with a 12 hr light cycle. All animals were maintained using standard procedures (Lenhoff & Brown, 1970). *Hydra* were fed freshly hatched, premium grade *Artemia nauplii* (https://www.brineshrimpdirect.com) 2-4 times a week and were transferred into fresh *Hydra* medium 4-8 hours after feeding. Animals were starved for at least 48 hours prior to experimentation.

Generation of transgenic strains

Transgenic strain *Tg(tba1c:mNeonGreen)*$^{cj1\text{-}gt}$ was made using a previously described protocol (Juliano, Lin, et al., 2014; Wittlieb et al., 2006). See Supplemental Material for details.

Preparation of cells for Fluorescence Activated Cell Sorting (FACS)

To prepare cells for FACS, transgenic *Hydra* from strains *Tg(actin1:GFP)*$^{rs3\text{-}in}$ and *Tg(tba1c:mNeonGreen)*$^{cj1\text{-}gt}$ were dissociated using Pronase E (VWR, E629-1G) as previously described (Siebert et al., 2019). See Supplemental Material for details.

10x Genomics Single Cell RNA Sequencing and Processing

Sorted transgenic *Hydra* cells were processed for sequencing using the Chromium Next GEM Single Cell 3' kit v3.1 (10x Genomics) according to manufacturer's instructions at the University of California, Davis Sequencing Core Facility. Data were aligned to the AEP genome assembly (Cazet et al., 2023) and were analyzed using previously described pipelines (Satija et al., 2015; Siebert et al., 2019). See Supplemental Material for details.

Generation of Differentiation Trajectories and Force Directed Layout

Differentiation trajectories and force directed layout were generated using previously described pipelines (Farrell et al., 2018; Siebert et al., 2019). See Supplemental Material for details.

ATAC-seq

ATAC-seq was performed on sorted, neuron enriched libraries using a previously described protocol (Cazet et al., 2023; Corces et al., 2017; Siebert et al., 2019). Data were aligned to the AEP genome assembly (Cazet et al. 2023) and were analyzed using a previously described pipeline (Cazet et al., 2023; Siebert et al., 2019). See Supplemental Material for details.

Whole Mount Double Fluorescent In Situ Hybridization

Whole-mount in situ hybridization was performed on strain AEP *H. vulgaris* using a previously described protocol (Siebert et al., 2019). See Supplemental Material for details.

ACKNOWLEDGEMENTS

We would like to thank Rob Steele for providing the *Tg(actin1:GFP)*$^{rs3\text{-}in}$ line, which was foundational to this study; the Juliano lab, Farrell lab, and David lab for invaluable discussions and feedback; Bruce Draper, Rob Steele, and Stefan Siebert for manuscript review and feedback; Clara Stuligross for analysis help, writing assistance, and moral support; Yohana Berhe for help with confocal images used in Fig S2; Diana Burkart-Waco, Siranoosh Ashtari, and Emily Kumimoto from from the DNA Technologies and Expression Analysis Core at the UC Davis Genome Center (supported by NIH Shared Instrumentation Grant 1S10OD010786-01) for technical advice and assistance with library preparation and sequencing; Bridget McLaughlin and Jonathan Van Dyke from the UC Davis Flow Cytometry Shared Resource Laboratory (supported by NCI P30 CA093373 (Comprehensive Cancer Center), S10 OD018223 (Astrios Cell Sorter), S10 RR 026825 (Fortessa Cytometer), and NIH NCRR C06-RR12088 (Tupper Hall room 3425 sorting suite renovations)) for technical advice, assistance with FACS sorting, and good conversation. This work was supported by a National Institutes of Health (NIH) Grant R35 GM133689 (to CEJ), a W.M. Keck Foundation Grant (to CEJ) and a National Institutes of Health (NIH) Grant ZIAHD008997 (to JAF). ASP and HML were supported in part by an NIH T32 predoctoral training program in Molecular and Cellular Biology (GM007377).

AUTHOR CONTRIBUTIONS

ASP, JFC, JAF, and CEJ designed research; ASP, SM, and CND performed research; ASP, BDC, SM, and CND collected data; ASP, JFC, HML, SM, CND, and JAF analyzed data; ASP and CEJ wrote the initial manuscript draft, ASP, JFC, HML, BDC, CND, JAF, and CEJ reviewed and edited the manuscript; and CEJ, JAF acquired funding.

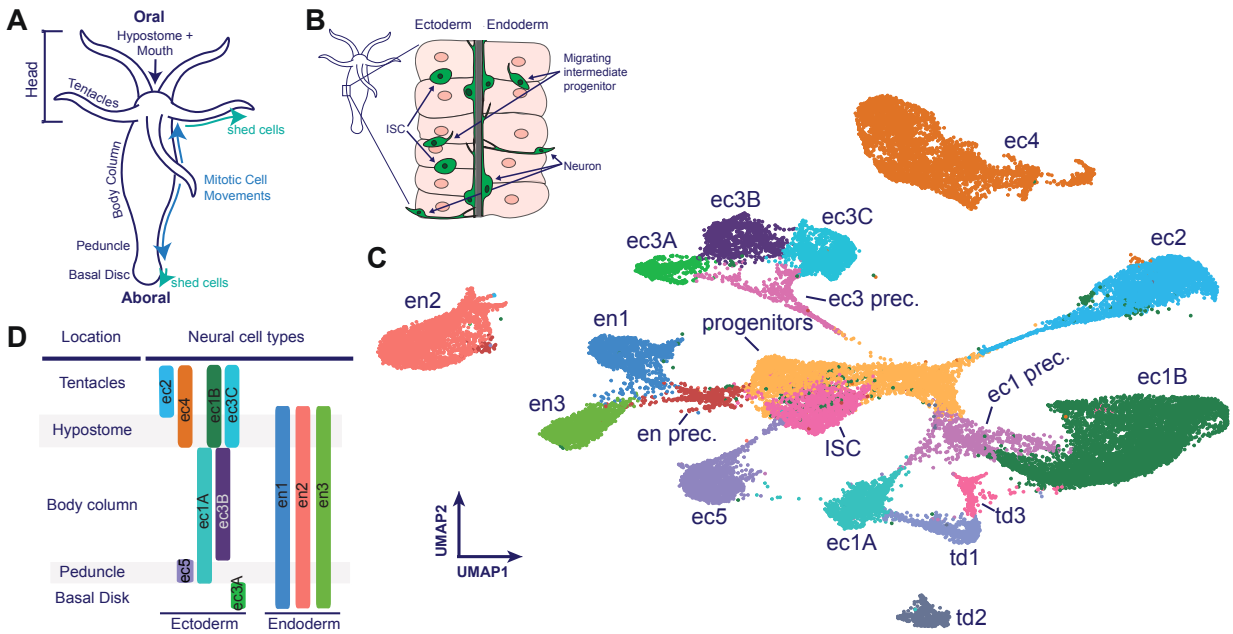

Figure 1. The *Hydra* vulgaris nervous system is composed of eleven transcriptionally distinct neuron subtypes. **(A)** The *Hydra* body is a radially symmetric hollow tube arranged around an oral-aboral axis. The hypostome, mouth, and tentacles (the "head") are located at the oral end and the peduncle and basal disk are located at the aboral end. These are connected by a body column consisting of dividing epithelial cells that generate passive tissue displacement towards the extremities, where the cells are eventually sloughed off (direction of tissue movement denoted with arrows). **(B)** *Hydra* consists of two epithelial cell layers, the endoderm and ectoderm, separated by an extracellular matrix (ECM). Neurons reside in the interstitial spaces of the epithelial cells to form two separate nerve nets, one in the ectodermal layer and one in the endodermal layer (Keramidioti et al., 2023). While the interstitial stem cells that give rise to neurons are found only in the ectoderm, intermediate neural progenitors migrate through the ECM to give rise to endodermal neuron subtypes. **(C)** 35,071 single cell transcriptomes were sequenced using a combination of Chromium Single- Cell Gene Expression (10x Genomics) (29,671 from this study) and Drop-Seq (5,400 from (Siebert et al., 2019)). UMAP representation of clustered cells annotated with cell state. ISC, interstitial stem cell; prec., precursors; ec, ectodermal; en, endodermal; td, transdifferentiation. The transdifferentiation clusters are likely intermediate states of transdifferentiation (see Fig. 5 for details) **(D)** Spatial location of the 11 neuron subtypes along the *Hydra* body. Colors match the clusters in Fig. 1C. Figure adapted from (Badhiwala et al., 2021) except that the ec1A spatial location has been adjusted to include the peduncle based on evidence provided by (Noro et al., 2019).

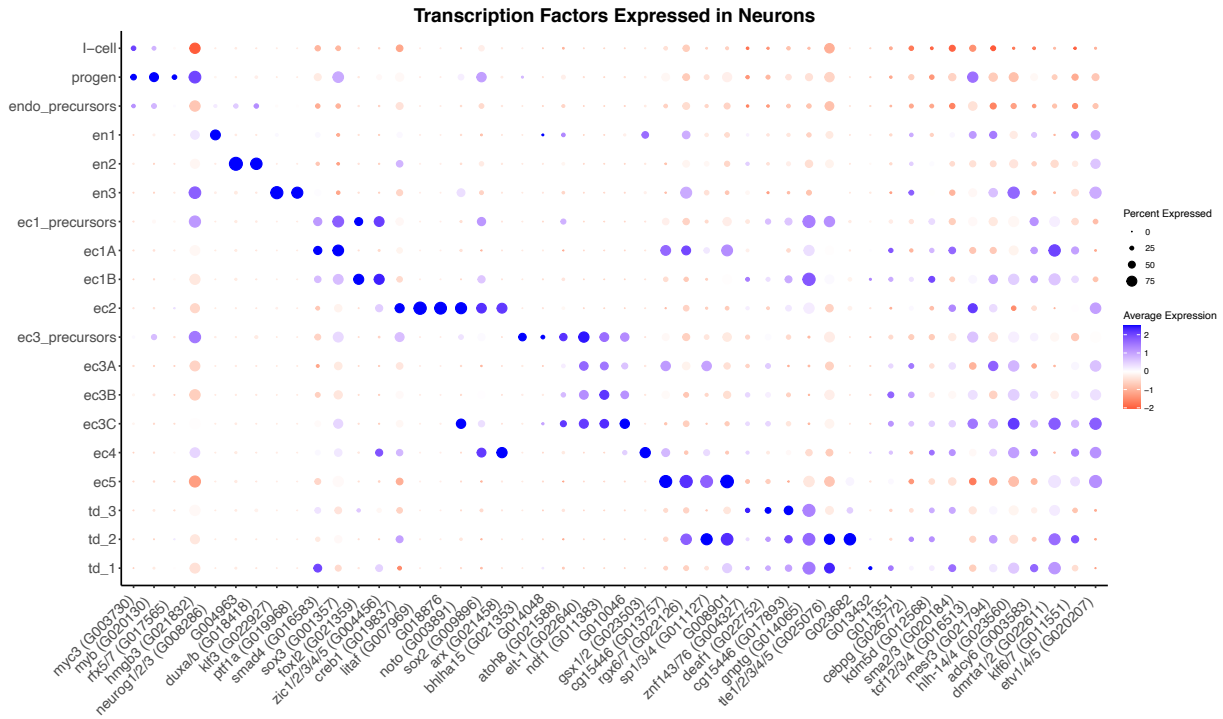

Figure 2. Forty-eight transcription factors (TFs) are specifically expressed in *Hydra* neurons. Dotplot representation of putative TFs uniquely expressed in the *Hydra* nervous system, including neuronal progenitor cells and each of *Hydra's* 11 neuron subtypes. Gene expression values are depicted by average expression across all cells (dot color) and percent expression within each cluster (dot size). Putative TFs were identified using PFAM annotations (data from (Cazet et al., 2023; Siebert et al., 2019)**.**

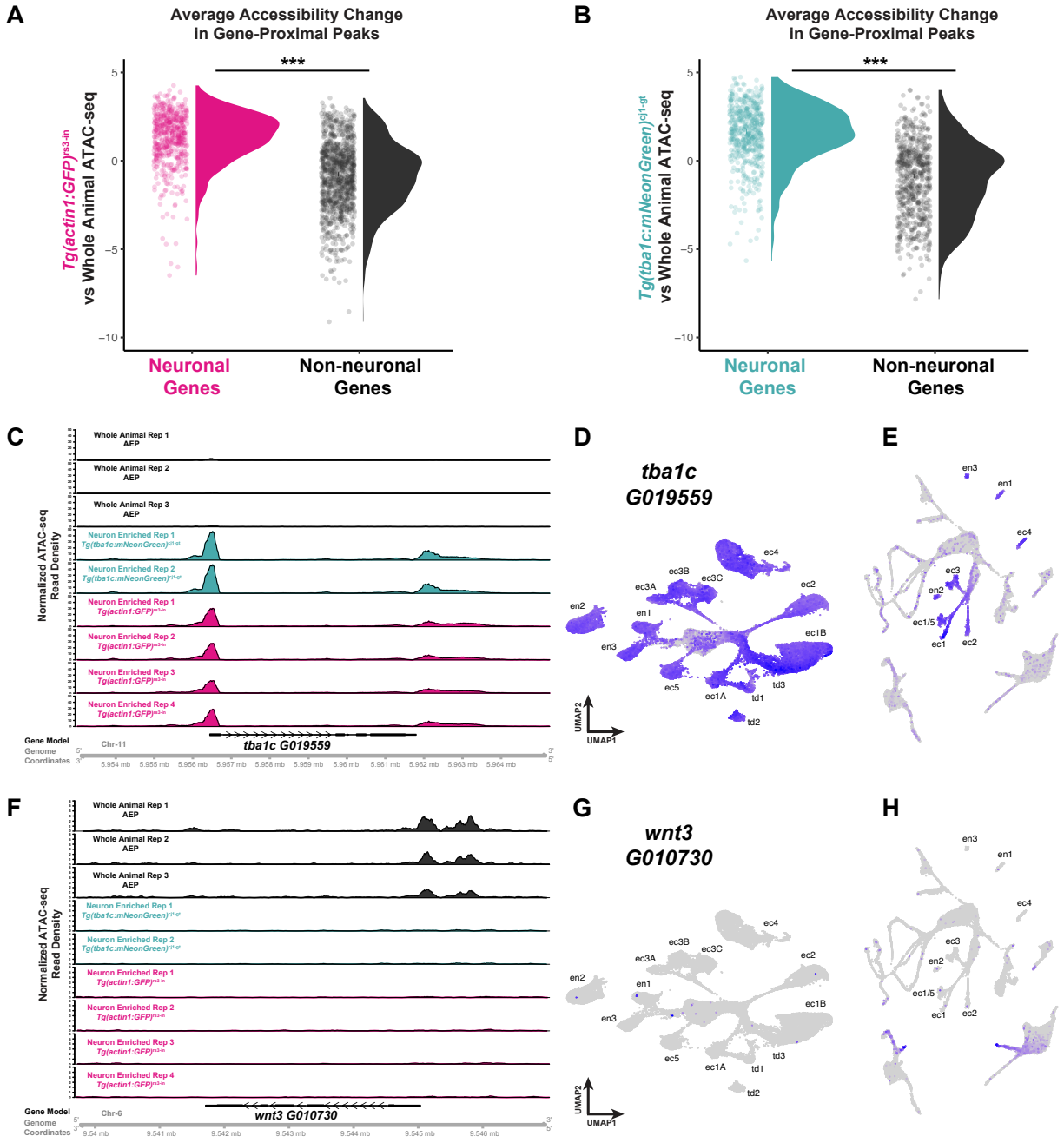

Figure 3. Characterization of the neuronal chromatin landscape using ATAC-seq. A total of six neuron-enriched ATAC-seq libraries were generated for this study: two from the *Tg(tba1c:mNeonGreen)*$^{cj1\text{-}gt}$ transgenic line and four from the *Tg(actin1:GFP)*$^{rs3\text{-}in}$ transgenic line (Keramidioti et al., 2023). Three whole animal ATAC-seq libraries (AEP1-3) were used from (Cazet et al., 2023) to test for enrichment of neuronal peaks in the neuron-enriched ATAC-seq libraries . **(A-B)** Average accessibility change in gene-proximal peaks in (A) *Tg(actin1:GFP)*$^{rs3\text{-}in}$ and (B) *Tg(tba1c:mNeonGreen)*$^{cj1\text{-}gt}$ as compared to whole animal AEP data sets. In both comparisons, there is significant enrichment ($p < 0.001$, t-test) of peaks within 10,000 base pairs of the transcription start site of neuronal genes as compared to non-neuronal genes. **(C-E)** Example (C) ATAC-seq data tracks and scRNA-seq expression data for the *alpha tubulin* gene (G019559) in (D) the neural UMAP (this study) and (E) in the previously published whole animal

data set (Cazet et al., 2023; Siebert et al., 2019). (D,E) *Alpha tubulin* has enriched expression in all neurons as compared to non-neuronal cell types. (C) Consistent with this, we observed ATAC-seq peaks enriched in the *Tg(tba1c:mNeonGreen)*$^{cj1\text{-}gt}$ (teal) and the *Tg(actin1:GFP)*$^{rs3\text{-}in}$ (magenta) libraries as compared to the whole animal libraries (black). **(F-H)** Example (F) ATAC-seq data tracks and (G,H) scRNA-seq expression data for the *wnt3* gene (G010730). *Wnt3* expression is largely restricted to epithelial cells at the oral end (Hobmayer et al., 2000) and is absent from neuronal cell types. Consistent with this, we observed ATAC-seq peaks enriched in the whole animal libraries (black) as compared to the *Tg(tba1c:mNeonGreen)*$^{cj1\text{-}gt}$ (teal) and *Tg(actin1:GFP)*$^{rs3\text{-}in}$ (magenta) libraries.

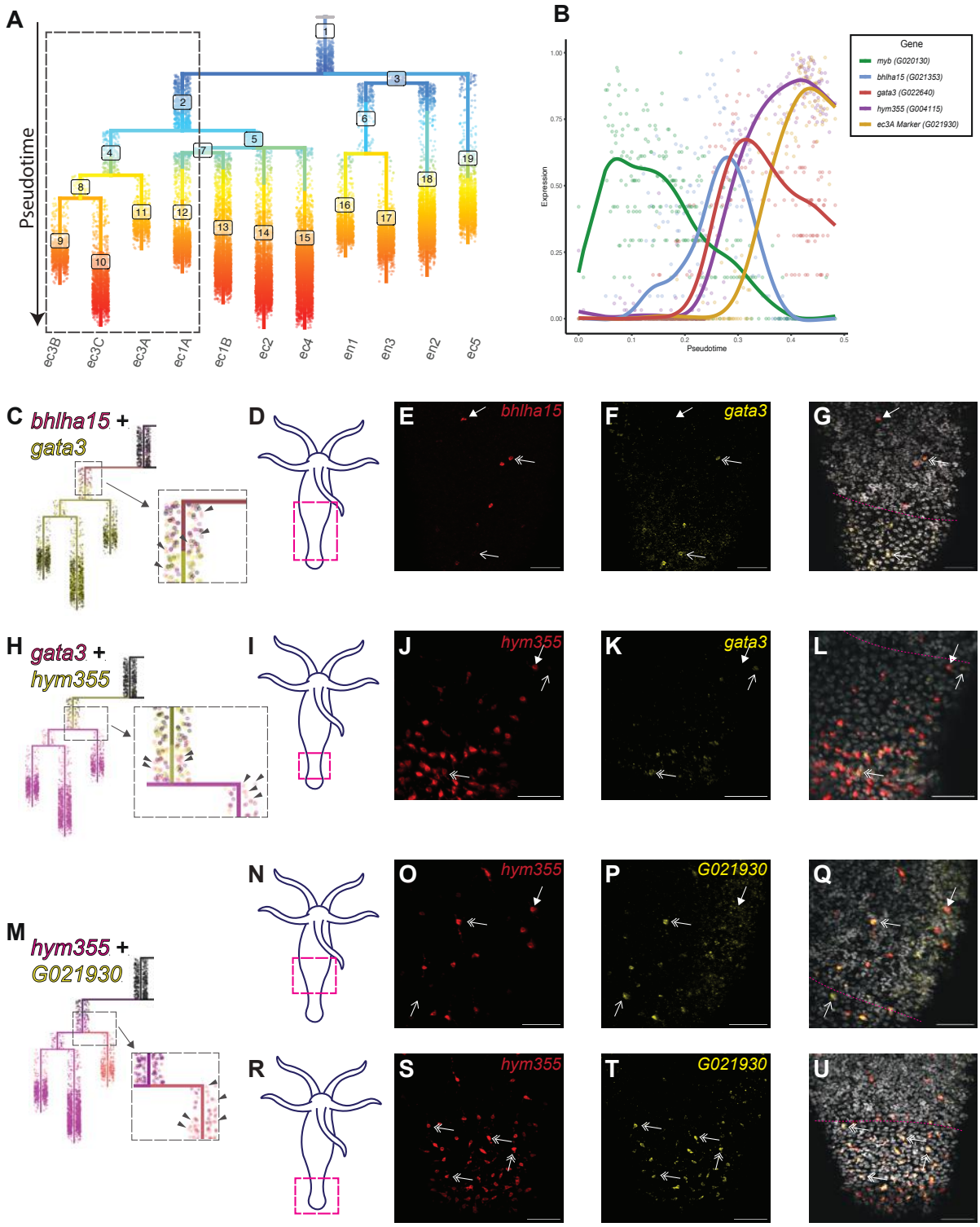

Fig 4. Trajectory reconstruction of *Hydra* neurogenesis indicates that ectodermal and endodermal neurons follow unique development pathways. **(A)** Differentiation trajectories describing the fate specification of *Hydra's* 11 neuron subtypes were reconstructed from the single cell data using URD (Farrell et al., 2018). Interstitial stem

cells were selected as the “root” or starting point of the tree and each neuron subtype was selected as a “tip”, or end of the tree. Tree is colored by pseudotime (developmental time), with earlier pseudotime at the top of the tree and later pseudotime at the bottom of the tree. Boxed area represents differentiation pathway validated in B-U. **(B)** Spline plot representation of five genes expressed during ec3A differentiation. Pseudotime is depicted on the X axis, with earlier pseudotime on the left and later pseudotime on the right. Gene expression levels are depicted on the Y axis. Each dot on the graph represents the average gene expression of 5 cells. **(C-U)** Validation of predicted transition states during differentiation of the ec3 subtypes using double fluorescent RNA *in situ* hybridization (FISH). Gene expression states in FISH images are indicated by the following arrow types: cells expressing only the first gene are depicted with a closed arrow, cells expressing only the second gene are depicted with an open arrow, and cells co-expressing both genes are depicted with a double arrow. **(C-G)** Validation of early ec3 differentiation transition states co-expressing *bhlha15* and *gata3*. **(C)** *bhlha15* (magenta) and *gata3* (yellow) gene expression visualized on the URD differentiation trajectory. Cells co-expressing genes are shown in orange and are indicated on the magnified section with arrow heads. Cells not expressing either gene are shown in black. **(D-G)** Confocal microscopy of double FISH. **(D)** Area on *Hydra* body imaged. Double FISH to identify **(E)** *bhlha15* (red) and **(F)** *gata3* (yellow) expressing cells. **(G)** The overlay shows nuclei labeled with Hoechst (gray). **(H-L)** Validation of mid ec3 differentiation transition states co-expressing *hym355* and *gata3*. **(H)** *hym355* (magenta) and *gata3* (yellow) gene expression visualized on the URD differentiation trajectory. Cells co-expressing genes are shown in orange and are indicated on the magnified section with arrow heads. Cells not expressing either gene are shown in black. **(I-L)** Confocal microscopy of double FISH. **(I)** Area on *Hydra* body imaged. Double FISH to identify **(J)** *hym355* (red) and **(K)** *gata3* (yellow) expressing cells. **(L)** The overlay shows nuclei labeled with Hoechst (gray). **(M-U)** Validation of late ec3 differentiation transition states co-expressing *hym355* and ec3A marker *G021930*. **(M)** *hym355* (magenta) and ec3A marker *G021930* (yellow) gene expression visualized on the URD differentiation trajectory. Cells co-expressing genes are shown in orange and are indicated on the magnified section with arrow heads. Cells not expressing either gene are shown in black. **(N-U)** Confocal microscopy of double FISH. **(N, R)** Areas on *Hydra* body imaged **(O, S)** *hym355* (red) and **(P, T)** ec3A marker (yellow) expressing cells. **(Q, U)** The overlay shows nuclei labeled with Hoechst (gray). Scale bar: 50 µm. Pink dotted line in microscopy images indicates the border between the body column and peduncle as determined by nuclei morphology.

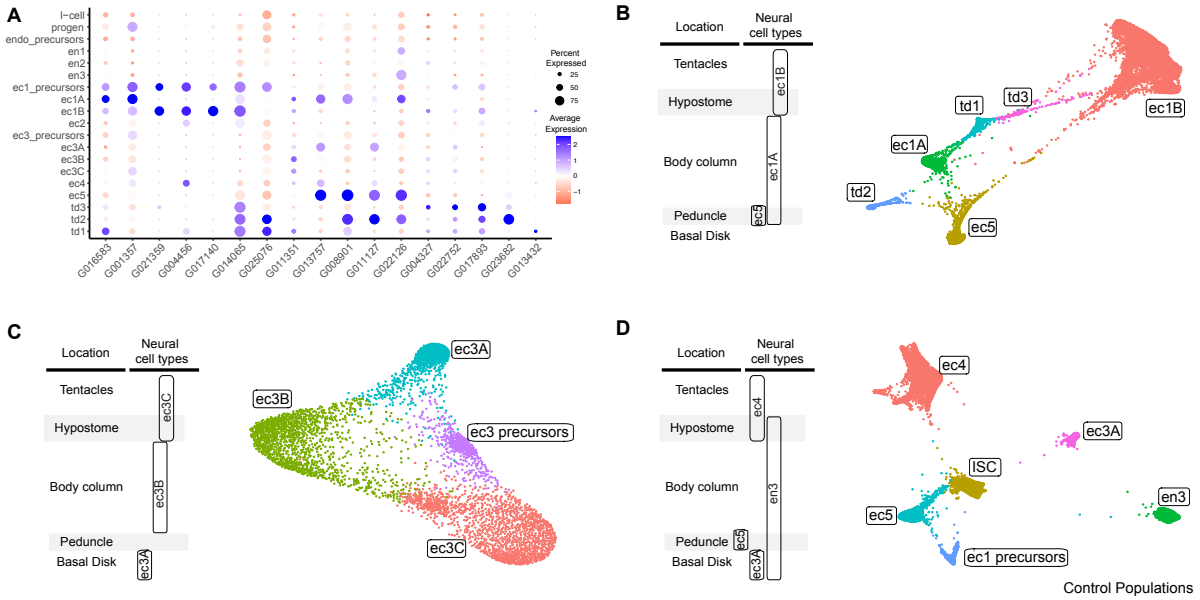

Fig 5. Force Directed Layout (FDL) demonstrates evidence of transdifferentiation between neuron subtypes. The neuron subtypes that could plausibly transdifferentiate were isolated and analyzed using FDL (Farrell et al., 2018; Fruchterman & Reingold, 1991). **(A)** Dotplot showing co-expression of markers between ec1A, ec1B, ec5, and td1-3. **(B)** FDL of subtypes ec1A, ec1B, ec5, td1, td2, td3 showing that ec1A (body column) connects to ec1B (hypostome/tentacles) through two intermediate transdifferentiation populations (td1 and td3). ec1A also appears to give rise to ec5 (peduncle) both directly and through an intermediate td2 population. **(C)** FDL of subtypes ec3A, ec3B, ec3C and ec3_precursors. ec3A (basal disk) and ec3C (hypostome/tentacles) appear to differentiate from ec3 precursors as well as transdifferentiate from ec3B (body column) neurons. **(D)** FDL control using populations (ec4, ec5, ec1 precursors, I-cell, ec3A, en3) with little to no predicted transcriptional similarity. Populations with more similar transcriptional profiles (I-cell, ec5, ec1 precursors) had stronger connections while populations with no similarity (ec4, ec3A, en3) had no connections.

REFERENCES

Abràmoff, D. M. D., Magalhães, P., & Ram, S. (2004). Image Processing with ImageJ. *Biophotonics International*, *11*(7), 36–42.

Albertin, C. B., Medina-Ruiz, S., Mitros, T., Schmidbaur, H., Sanchez, G., Wang, Z. Y., Grimwood, J., Rosenthal, J. J. C., Ragsdale, C. W., Simakov, O., & Rokhsar, D. S. (2022). Genome and transcriptome mechanisms driving cephalopod evolution. *Nature Communications*, *13*(1), Article 1. https://doi.org/10.1038/s41467-022-29748-w

Angerer, P., Haghverdi, L., Büttner, M., Theis, F. J., Marr, C., & Buettner, F. (2016). destiny: Diffusion maps for large-scale single-cell data in R. *Bioinformatics*, *32*(8), 1241–1243. https://doi.org/10.1093/bioinformatics/btv715

Badhiwala, K. N., Primack, A. S., Juliano, C. E., & Robinson, J. T. (2021). Multiple neuronal networks coordinate Hydra mechanosensory behavior. *ELife*, *10*, e64108. https://doi.org/10.7554/eLife.64108

Blader, P., Fischer, N., Gradwohl, G., Guillemot, F., & Strähle, U. (1997). The activity of Neurogenin1 is controlled by local cues in the zebrafish embryo. *Development*, *124*(22), 4557–4569. https://doi.org/10.1242/dev.124.22.4557

Bode, H., Berking, S., David, C. N., Gierer, A., Schaller, H., & Trenkner, E. (1973). Quantitative analysis of cell types during growth and morphogenesis in Hydra. *Wilhelm Roux Archiv F⍰r Entwicklungsmechanik Der Organismen*, *171*(4), 269–285. https://doi.org/10.1007/BF00577725

Bode, H. R. (1992). Continuous conversion of neuron phenotype in hydra. *Trends in Genetics*, *8*(8), 279–284. https://doi.org/10.1016/0168-9525(92)90254-2

Bode, H. R., Heimfeld, S., Koizumi, O., LlTTLEFIELD, C. L., & Yaross, M. S. (1988). Maintenance and Regeneration of the Nerve Net in Hydra. *American Zoologist*, *28*(4), 1053–1063. https://doi.org/10.1093/icb/28.4.1053

Bolger, A. M., Lohse, M., & Usadel, B. (2014). Trimmomatic: A flexible trimmer for Illumina sequence data. *Bioinformatics*, *30*(15), 2114–2120. https://doi.org/10.1093/bioinformatics/btu170

Buenrostro, J. D., Giresi, P. G., Zaba, L. C., Chang, H. Y., & Greenleaf, W. J. (2013). Transposition of native chromatin for fast and sensitive epigenomic profiling of open chromatin, DNA-binding proteins and nucleosome position. *Nature Methods*, *10*(12), Article 12. https://doi.org/10.1038/nmeth.2688

Butler, A., Hoffman, P., Smibert, P., Papalexi, E., & Satija, R. (2018). Integrating single-cell transcriptomic

data across different conditions, technologies, and species. *Nature Biotechnology*, *36*(5), Article 5. https://doi.org/10.1038/nbt.4096

Bylund, M., Andersson, E., Novitch, B. G., & Muhr, J. (2003). Vertebrate neurogenesis is counteracted by Sox1–3 activity. *Nature Neuroscience*, *6*(11), Article 11. https://doi.org/10.1038/nn1131

Campbell, R. D. (1967). Tissue dynamics of steady state growth inHydra littoralis. II. Patterns of tissue movement. *Journal of Morphology*, *121*(1), 19–28. https://doi.org/10.1002/jmor.1051210103

Cazet, J. F., Siebert, S., Morris Little, H., Bertemes, P., Primack, A. S., Ladurner, P., Achrainer, M., Fredriksen, M. T., Moreland, R. T., Singh, S., Zhang, S., Wolfsberg, T. G., Schnitzler, C. E., Baxevanis, A. D., Simakov, O., Hobmayer, B., & Juliano, C. E. (2023). A chromosome-scale epigenetic map of the *Hydra* genome reveals conserved regulators of cell state. *Genome Research*, gr.277040.122. https://doi.org/10.1101/gr.277040.122

Corces, M. R., Trevino, A. E., Hamilton, E. G., Greenside, P. G., Sinnott-Armstrong, N. A., Vesuna, S., Satpathy, A. T., Rubin, A. J., Montine, K. S., Wu, B., Kathiria, A., Cho, S. W., Mumbach, M. R., Carter, A. C., Kasowski, M., Orloff, L. A., Risca, V. I., Kundaje, A., Khavari, P. A., … Chang, H. Y. (2017). An improved ATAC-seq protocol reduces background and enables interrogation of frozen tissues. *Nature Methods*, *14*(10), Article 10. https://doi.org/10.1038/nmeth.4396

David, C. N. (2012). Interstitial stem cells in Hydra: Multipotency and decision-making. *The International Journal of Developmental Biology*, *56*(6-7–8), 489–497. https://doi.org/10.1387/ijdb.113476cd

David, C. N., & Gierer, A. (1974). *Cell Cycle Kinetics and Development of Hydra attenuata. III. Nerve and nematocyte differentiation.*

David, C. N., & Murphy, S. (1977). Characterization of interstitial stem cells in hydra by cloning. *Developmental Biology*, *58*, 372–383.

Doitsidou, M., Minevich, G., Kroll, J. R., Soete, G., Gowtham, S., Korswagen, H. C., Zon, J. S. van, & Hobert, O. (2018). A Caenorhabditis elegans Zinc Finger Transcription Factor, ztf-6, Required for the Specification of a Dopamine Neuron-Producing Lineage. *G3: Genes, Genomes, Genetics*, *8*(1), 17–26. https://doi.org/10.1534/g3.117.300132

Dupre, C., & Yuste, R. (2017). Non-overlapping Neural Networks in Hydra vulgaris. *Current Biology*, *27*(8), 1085–1097. https://doi.org/10.1016/j.cub.2017.02.049

Dworkin, S., Heath, J. K., deJong-Curtain, T. A., Hogan, B. M., Lieschke, G. J., Malaterre, J., Ramsay, R. G., & Mantamadiotis, T. (2007). CREB activity modulates neural cell proliferation, midbrain–hindbrain organization and patterning in zebrafish. *Developmental Biology*, *307*(1), 127–141. https://doi.org/10.1016/j.ydbio.2007.04.026

Farrell, J. A., Wang, Y., Riesenfeld, S. J., Shekhar, K., Regev, A., & Schier, A. F. (2018). Single-cell reconstruction of developmental trajectories during zebrafish embryogenesis. *Science*, *360*(6392), eaar3131. https://doi.org/10.1126/science.aar3131

Fincher, C. T., Wurtzel, O., de Hoog, T., Kravarik, K. M., & Reddien, P. W. (2018). Cell type transcriptome atlas for the planarian *Schmidtea mediterranea*. *Science*, *360*(6391), eaaq1736. https://doi.org/10.1126/science.aaq1736

Fruchterman, T. M. J., & Reingold, E. M. (1991). Graph drawing by force-directed placement. *Software: Practice and Experience*, *21*(11), 1129–1164. https://doi.org/10.1002/spe.4380211102

Hafemeister, C., & Satija, R. (2019). Normalization and variance stabilization of single-cell RNA-seq data using regularized negative binomial regression. *Genome Biology*, *20*(1), 296. https://doi.org/10.1186/s13059-019-1874-1

Hager, G., & David, C. N. (1997). Pattern of differentiated nerve cells in hydra is determined by precursor migration. *Development*, *124*(2), 569–576.

Hahne, F., & Ivanek, R. (2016). Visualizing Genomic Data Using Gviz and Bioconductor. *Methods in Molecular Biology (Clifton, N.J.)*, *1418*, 335–351. https://doi.org/10.1007/978-1-4939-3578-9_16

Hao, Y., Hao, S., Andersen-Nissen, E., Mauck, W. M., Zheng, S., Butler, A., Lee, M. J., Wilk, A. J., Darby, C., Zager, M., Hoffman, P., Stoeckius, M., Papalexi, E., Mimitou, E. P., Jain, J., Srivastava, A., Stuart, T., Fleming, L. M., Yeung, B., … Satija, R. (2021). Integrated analysis of multimodal single-cell data. *Cell*, *184*(13), 3573-3587.e29. https://doi.org/10.1016/j.cell.2021.04.048

Hobert, O. (2016). Chapter Twenty-Five—Terminal Selectors of Neuronal Identity. In P. M. Wassarman (Ed.), *Current Topics in Developmental Biology* (Vol. 116, pp. 455–475). Academic Press. https://doi.org/10.1016/bs.ctdb.2015.12.007

Hobmayer, B., Rentzsch, F., Kuhn, K., Happel, C. M., von Laue, C. C., Snyder, P., Rothbächer, U., & Holstein, T. W. (2000). WNT signalling molecules act in axis formation in the diploblastic metazoan Hydra. *Nature*, *407*(6801), 186–189. https://doi.org/10.1038/35025063

Hulett, R. E., Kimura, J. O., Bolaños, D. M., Luo, Y.-J., Ricci, L., & Srivastava, M. (2022). *Acoel single-cell atlas reveals expression dynamics and heterogeneity of a pluripotent stem cell population* [Preprint]. Developmental Biology. https://doi.org/10.1101/2022.02.10.479464

Hulett, R. E., Potter, D., & Srivastava, M. (2020). Neural architecture and regeneration in the acoel Hofstenia miamia. *Proceedings of the Royal Society B: Biological Sciences*, *287*(1931), 20201198. https://doi.org/10.1098/rspb.2020.1198

Jacomy, M., Venturini, T., Heymann, S., & Bastian, M. (2014). ForceAtlas2, a Continuous Graph Layout

Algorithm for Handy Network Visualization Designed for the Gephi Software. *PLOS ONE*, *9*(6), e98679. https://doi.org/10.1371/journal.pone.0098679

Jarman, A. P., Grau, Y., Jan, L. Y., & Jan, Y. N. (1993). Atonal is a proneural gene that directs chordotonal organ formation in the Drosophila peripheral nervous system. *Cell*, *73*(7), 1307–1321. https://doi.org/10.1016/0092-8674(93)90358-W

Juliano, C. E., Lin, H., & Steele, R. E. (2014). Generation of Transgenic Hydra by Embryo Microinjection. *JoVE (Journal of Visualized Experiments)*, *91*, e51888. https://doi.org/10.3791/51888

Juliano, C. E., Reich, A., Liu, N., Götzfried, J., Zhong, M., Uman, S., Reenan, R. A., Wessel, G. M., Steele, R. E., & Lin, H. (2014). PIWI proteins and PIWI-interacting RNAs function in Hydra somatic stem cells. *Proceedings of the National Academy of Sciences of the United States of America*, *111*(1), 337–342. https://doi.org/10.1073/pnas.1320965111

Keramidioti, A., Schneid, S., Busse, C., Laue, C. C. von, Bertulat, B., Salvenmoser, W., Hess, M., Alexandrova, O., Glauber, K., Steele, R., Hobmayer, B., Holstein, T. W., & David, C. N. (2023). *A new look at the architecture and dynamics of the Hydra nerve net* (p. 2023.02.22.529525). bioRxiv. https://doi.org/10.1101/2023.02.22.529525

Klimovich, A., Giacomello, S., Björklund, Å., Faure, L., Kaucka, M., Giez, C., Murillo-Rincon, A. P., Matt, A.-S., Willoweit-Ohl, D., Crupi, G., de Anda, J., Wong, G. C. L., D'Amato, M., Adameyko, I., & Bosch, T. C. G. (2020). Prototypical pacemaker neurons interact with the resident microbiota. *Proceedings of the National Academy of Sciences*, *117*(30), 17854–17863. https://doi.org/10.1073/pnas.1920469117

Klimovich, A., Wittlieb, J., & Bosch, T. C. G. (2019). Transgenesis in Hydra to characterize gene function and visualize cell behavior. *Nature Protocols*, *14*(7), Article 7. https://doi.org/10.1038/s41596-019-0173-3

Knoepfler, P. S., Cheng, P. F., & Eisenman, R. N. (2002). N-myc is essential during neurogenesis for the rapid expansion of progenitor cell populations and the inhibition of neuronal differentiation. *Genes & Development*, *16*(20), 2699–2712. https://doi.org/10.1101/gad.1021202

Koizumi, O., & Bode, H. R. (1986). Plasticity in the nervous system of adult hydra: I. The position-dependent expression of FMRFamide-like immunoreactivity. *Developmental Biology*, *116*(2), 407–421. https://doi.org/10.1016/0012-1606(86)90142-9

Koizumi, O., & Bode, H. R. (1991). Plasticity in the nervous system of adult hydra. III. Conversion of neurons to expression of a vasopressin-like immunoreactivity depends on axial location. *Journal of Neuroscience*, *11*(7), 2011–2020. https://doi.org/10.1523/JNEUROSCI.11-07-02011.1991

Koizumi, O., Heimfeld, S., & Bode, H. R. (1988). Plasticity in the nervous system of adult hydra: II. Conversion of ganglion cells of the body column into epidermal sensory cells of the hypostome. *Developmental Biology*, *129*(2), 358–371. https://doi.org/10.1016/0012-1606(88)90383-1

Kondili, M., Fust, A., Preussner, J., Kuenne, C., Braun, T., & Looso, M. (2017). UROPA: A tool for Universal RObust Peak Annotation. *Scientific Reports*, *7*(1), 2593. https://doi.org/10.1038/s41598-017-02464-y

Kotliar, D., Veres, A., Nagy, M. A., Tabrizi, S., Hodis, E., Melton, D. A., & Sabeti, P. C. (2019). Identifying gene expression programs of cell-type identity and cellular activity with single-cell RNA-Seq. *ELife*, *8*, e43803. https://doi.org/10.7554/eLife.43803

Landt, S. G., Marinov, G. K., Kundaje, A., Kheradpour, P., Pauli, F., Batzoglou, S., Bernstein, B. E., Bickel, P., Brown, J. B., Cayting, P., Chen, Y., DeSalvo, G., Epstein, C., Fisher-Aylor, K. I., Euskirchen, G., Gerstein, M., Gertz, J., Hartemink, A. J., Hoffman, M. M., … Snyder, M. (2012). ChIP-seq guidelines and practices of the ENCODE and modENCODE consortia. *Genome Research*, *22*(9), 1813–1831. https://doi.org/10.1101/gr.136184.111

Langmead, B., & Salzberg, S. L. (2012). Fast gapped-read alignment with Bowtie 2. *Nature Methods*, *9*(4), Article 4. https://doi.org/10.1038/nmeth.1923

Lee, J. E. (1997). Basic helix-loop-helix genes in neural development. *Current Opinion in Neurobiology*, *7*, 13–20.

Lee, J. E., Hollenberg, S. M., Snider, L., Turner, D. L., Lipnick, N., & Weintraub, H. (1995). Conversion of *Xenopus* Ectoderm into Neurons by NeuroD, a Basic Helix-Loop-Helix Protein. *Science*, *268*(5212), 836–844. https://doi.org/10.1126/science.7754368

Lenhoff, H. M., & Brown, R. D. (1970). Mass culture of hydra: An improved method and its application to other aquatic invertebrates. *Laboratory Animals*, *4*(1), 139–154. https://doi.org/10.1258/002367770781036463

Li, H., Handsaker, B., Wysoker, A., Fennell, T., Ruan, J., Homer, N., Marth, G., Abecasis, G., Durbin, R., & 1000 Genome Project Data Processing Subgroup. (2009). The Sequence Alignment/Map format and SAMtools. *Bioinformatics*, *25*(16), 2078–2079. https://doi.org/10.1093/bioinformatics/btp352

Li, Q., Brown, J. B., Huang, H., & Bickel, P. J. (2011). Measuring reproducibility of high-throughput experiments. *The Annals of Applied Statistics*, *5*(3). https://doi.org/10.1214/11-AOAS466

Lohmann, J. U., Endl, I., & Bosch, T. C. G. (1999). Silencing of Developmental Genes in Hydra. *Developmental Biology*, *214*(1), 211–214. https://doi.org/10.1006/dbio.1999.9407

Macosko, E. Z., Basu, A., Satija, R., Nemesh, J., Shekhar, K., Goldman, M., Tirosh, I., Bialas, A. R., Kamitaki, N., Martersteck, E. M., Trombetta, J. J., Weitz, D. A., Sanes, J. R., Shalek, A. K., Regev, A., & McCarroll, S. A. (2015). Highly Parallel Genome-wide Expression Profiling of Individual Cells Using Nanoliter Droplets. *Cell*, *161*(5), 1202–1214. https://doi.org/10.1016/j.cell.2015.05.002

McInnes, L., Healy, J., Saul, N., & Großberger, L. (2018). UMAP: Uniform Manifold Approximation and Projection. *Journal of Open Source Software*, *3*(29), 861. https://doi.org/10.21105/joss.00861

Miyata, T., Maeda, T., & Lee, J. E. (1999). NeuroD is required for differentiation of the granule cells in the cerebellum and hippocampus. *Genes & Development*, *13*(13), 1647–1652.

Noro, Y., Yum, S., Nishimiya-Fujisawa, C., Busse, C., Shimizu, H., Mineta, K., Zhang, X., Holstein, T. W., David, C. N., Gojobori, T., & Fujisawa, T. (2019). Regionalized nervous system in Hydra and the mechanism of its development. *Gene Expression Patterns*, *31*, 42–59. https://doi.org/10.1016/j.gep.2019.01.003

Orvis, J., Albertin, C. B., Shrestha, P., Chen, S., Zheng, M., Rodriguez, C. J., Tallon, L. J., Mahurkar, A., Zimin, A. V., Kim, M., Liu, K., Kandel, E. R., Fraser, C. M., Sossin, W., & Abrams, T. W. (2022). The evolution of synaptic and cognitive capacity: Insights from the nervous system transcriptome of *Aplysia*. *Proceedings of the National Academy of Sciences*, *119*(28), e2122301119. https://doi.org/10.1073/pnas.2122301119

Patel, T., & Hobert, O. (2017). Coordinated control of terminal differentiation and restriction of cellular plasticity. *ELife*, *6*. https://doi.org/10.7554/eLife.24100

Ramírez, F., Ryan, D. P., Grüning, B., Bhardwaj, V., Kilpert, F., Richter, A. S., Heyne, S., Dündar, F., & Manke, T. (2016). deepTools2: A next generation web server for deep-sequencing data analysis. *Nucleic Acids Research*, *44*(W1), W160–W165. https://doi.org/10.1093/nar/gkw257

Rogers, N., Cheah, P.-S., Szarek, E., Banerjee, K., Schwartz, J., & Thomas, P. (2013). Expression of the murine transcription factor SOX3 during embryonic and adult neurogenesis. *Gene Expression Patterns*, *13*(7), 240–248. https://doi.org/10.1016/j.gep.2013.04.004

Sachkova, M. Y., Nordmann, E.-L., Soto-Àngel, J. J., Meeda, Y., Górski, B., Naumann, B., Dondorp, D., Chatzigeorgiou, M., Kittelmann, M., & Burkhardt, P. (2021). Neuropeptide repertoire and 3D anatomy of the ctenophore nervous system. *Current Biology*, *31*(23), 5274-5285.e6. https://doi.org/10.1016/j.cub.2021.09.005

Satija, R., Farrell, J. A., Gennert, D., Schier, A. F., & Regev, A. (2015). Spatial reconstruction of single-cell gene expression data. *Nature Biotechnology*, *33*(5), Article 5. https://doi.org/10.1038/nbt.3192

Sebé-Pedrós, A., Saudemont, B., Chomsky, E., Plessier, F., Mailhé, M.-P., Renno, J., Loe-Mie, Y., Lifshitz,

A., Mukamel, Z., Schmutz, S., Novault, S., Steinmetz, P. R. H., Spitz, F., Tanay, A., & Marlow, H. (2018). Cnidarian Cell Type Diversity and Regulation Revealed by Whole-Organism Single-Cell RNA-Seq. *Cell*, *173*(6), 1520-1534.e20. https://doi.org/10.1016/j.cell.2018.05.019

Siebert, S., Farrell, J. A., Cazet, J. F., Abeykoon, Y., Primack, A. S., Schnitzler, C. E., & Juliano, C. E. (2019). Stem cell differentiation trajectories in Hydra resolved at single-cell resolution. *Science*, *365*(6451). https://doi.org/10.1126/science.aav9314

Stuart, T., Butler, A., Hoffman, P., Hafemeister, C., Papalexi, E., Mauck, W. M., Hao, Y., Stoeckius, M., Smibert, P., & Satija, R. (2019). Comprehensive Integration of Single-Cell Data. *Cell*, *177*(7), 1888-1902.e21. https://doi.org/10.1016/j.cell.2019.05.031

Vogg, M. C., Ferenc, J., Buzgariu, W. C., Perruchoud, C., Sanchez, P. G. L., Beccari, L., Nuninger, C., Le Cras, Y., Delucinge-Vivier, C., Papasaikas, P., Vincent, S., Galliot, B., & Tsiairis, C. D. (2022). The transcription factor Zic4 promotes tentacle formation and prevents epithelial transdifferentiation in Hydra. *Science Advances*, *8*(51), eabo0694. https://doi.org/10.1126/sciadv.abo0694

Wittlieb, J., Khalturin, K., Lohmann, J. U., Anton-Erxleben, F., & Bosch, T. C. G. (2006). Transgenic Hydra allow in vivo tracking of individual stem cells during morphogenesis. *Proceedings of the National Academy of Sciences*, *103*(16), 6208–6211. https://doi.org/10.1073/pnas.0510163103

Zhang, Y., Liu, T., Meyer, C. A., Eeckhoute, J., Johnson, D. S., Bernstein, B. E., Nusbaum, C., Myers, R. M., Brown, M., Li, W., & Liu, X. S. (2008). Model-based Analysis of ChIP-Seq (MACS). *Genome Biology*, *9*(9), R137. https://doi.org/10.1186/gb-2008-9-9-r137